Integrative Biology

PAPER

Cite this: *Integr. Biol.*, 2018, **10**, 174

A three-dimensional *in vitro* dynamic micro-tissue model of cardiac scar formation†

Paola Occhetta,‡[ab] Giuseppe Isu,‡[ab] Marta Lemme,§[abc] Chiara Conficconi,[abc] Philipp Oertle,[d] Christian Räz,[d] Roberta Visone,[c] Giulia Cerino,[ab] Marija Plodinec,[d] Marco Rasponi[c] and Anna Marsano*[ab]

Received 21st November 2017,
Accepted 28th February 2018

DOI: 10.1039/c7ib00199a

rsc.li/integrative-biology

In vitro cardiac models able to mimic the fibrotic process are paramount to develop an effective anti-fibrosis therapy that can regulate fibroblast behaviour upon myocardial injury. In previously developed *in vitro* models, typical fibrosis features were induced by using scar-like stiffness substrates and/or potent morphogen supplementation in monolayer cultures. In our model, we aimed to mimic *in vitro* a fibrosis-like environment by applying cyclic stretching of cardiac fibroblasts embedded in three-dimensional fibrin-hydrogels alone. Using a microfluidic device capable of delivering controlled cyclic mechanical stretching (10% strain at 1 Hz), some of the main fibrosis hallmarks were successfully reproduced in 7 days. Cyclic strain indeed increased cell proliferation, extracellular matrix (ECM) deposition (*e.g.* type-I-collagen, fibronectin) and its stiffness, forming a scar-like tissue with superior quality compared to the supplementation of TGFβ1 alone. Taken together, the observed findings resemble some of the key steps in the formation of a scar: (i) early fibroblast proliferation, (ii) later phenotype switch into myofibroblasts, (iii) ECM deposition and (iv) stiffening. This *in vitro* scar-on-a-chip model represents a big step forward to investigate the early mechanisms possibly leading later to fibrosis without any possible confounding supplementation of exogenous potent morphogens.

Insight, innovation, integration

Since no treatment is currently available for cardiac fibrosis, the development of *in vitro* scar-models is crucial for identifying possible therapeutic molecular targets. Previous models, mainly two-dimensional cell cultures, only partially reproduced the disease using either scar-like-stiff substrates and/or potent morphogen supplementation at supra-physiological doses. The *scar-on-chip* model proposed here mimics some of the key steps of scar formation (fibroblast proliferation and activation, extracellular matrix remodeling and stiffening) by the sole application of mechanical stimulation on muscle-like-soft three-dimensional cardiac fibroblast-laden hydrogels (reducing possible confounding effects of exogenous morphogens). Given the presented key biological initial findings, this *scar-on-chip* tissue model offers a promising future tool for biological discovery thanks to the fine integration of innovative microfluidic and microscopy technologies.

1. Introduction

Following a myocardial infarction, the heart undergoes a strong healing process intertwined with ventricular remodeling. Scar formation is a natural step of the wound healing process, which occurs to prevent myocardial rupture and to stabilize the cardiac output. However, an excessive deposition of extracellular matrix (ECM) (namely, fibrosis) significantly reduces the organ function and might lead to heart failure. An effective treatment for cardiac fibrosis is not yet available, since it is a dynamic process, in which the key role of fibroblast activation and differentiation still needs to be elucidated.[1] During the normal wound healing, fibroblasts, both resident and the ones migrating towards the injury site, change their status from quiescent to activated. Activated fibroblasts proliferate, produce stress fibers and differentiate into myofibroblasts, increasing the deposition and formation of a stiffer-scar tissue. Myofibroblasts are indeed characterized by enhanced expression of particular contractile proteins (*e.g.* α-smooth muscle actin (SMA), vimentin) and structural ECM proteins (*e.g.* types I

[a] *Department of Biomedicine, University of Basel, Hebelstrasse 20, CH-4031 Basel, Switzerland. E-mail: Anna.Marsano@usb.ch; Tel: +41 (0)61 265 2979*
[b] *Department of Surgery, University Hospital Basel, Basel, Switzerland*
[c] *Department of Electronics, Information and Bioengineering, Politecnico di Milano, Piazza Leonardo da Vinci 32, Building #21, 20133 Milano, Italy*
[d] *Biozentrum and the Swiss Nanoscience Institute, University of Basel, 4056 Basel, Switzerland*

† Electronic supplementary information (ESI) available. See DOI: 10.1039/c7ib00199a

‡ Equally contributed.

§ Current address: Department of Experimental Pharmacology and Toxicology, Cardiovascular Research Center, University Medical Center Hamburg-Eppendorf, Germany.

and III collagen, fibronectin).[2] *In vitro* fibrosis models offer the opportunity to understand the main mechanisms behind fibroblast behavior in a standard and clear environment without multiple confounding variables (*e.g.* chronic inflammation) typical of an *in vivo* setting. Indeed, although Sonin *et al.*[3] investigated the effects of inhibition of the thrombin receptor, in an *in vivo* cardiac fibrosis model, they also needed an *in vitro* culture to specifically elucidate its role in thrombin-induced TGF-β and ERK 1/2 activities in cardiac fibroblasts. The currently developed *in vitro* fibrosis models reproduced some key aspects of the disease such as hypoxic condition,[4] scar-like substrate stiffness[5,6] and static[5] or cyclic stretching.[7] The *in vitro* fibroblast activation and their phenotypic switch into myofibroblasts are indeed often induced upon biochemical and mechanical stimuli (in particular using two-dimensional (2D) scar-like stiff substrates).[8–10] Among the numerous regulators of fibroblasts (*e.g.* angiotensin-II, endothelin-1, and basic fibroblast growth factor),[11,12] TGFβ-1 is considered pivotal to activate myofibroblasts in various organs including the heart[8,13] and it is often used as a unique triggering factor to mimic a fibrotic environment *in vitro*.[7,9] While substrate stiffness alone was also shown to regulate the fate of fibroblasts by mainly promoting fiber formation (*e.g.* expression of stress fibers), external mechanical stretching regulates instead expression of α-SMA and types I and III collagen deposition. However, in 2D culture environments, the effect of external static stretching depends on the chosen substrate stiffness and it seemed to induce fibrotic gene and protein expression only when a scar-like substrate (∼30 kPa) is used.[14] Starting from the muscle-like stiffness range (3–10 kPa), the effects of static mechanical stretching on pro-fibrotic switch were indeed less evident.[5] Although 2D *in vitro* models of fibrosis offer a good control over culture substrate stiffness, they cannot mimic the complexity of the native, three-dimensional (3D) environment characterized by cell–cell and cell–matrix interactions.[15,16] Microfluidic technologies had also recently enabled the development of advanced cardiac models by integrating key environmental features within cardiac cell culture systems.[4,17] In this study, we proposed an *in vitro* 3D micro-scale cardiac-scar tissue model by the imposition of cyclic mechanical stimulation and by the supplementation of specific biochemical factors (TGFβ1) in a recently developed microdevice platform. In particular, our aim was to recapitulate the early stage fibroblast activation and transition to myofibroblasts, and the initial ECM deposition and stiffening using cyclic mechanical stretching. We hypothesize that cyclic stretching alone can recapitulate *in vitro* the key steps of the initial scar formation in a soft 3D substrate.

2. Experimental

2.1 Microfluidic device concept and fabrication

The designed microfluidic device is composed of two compartments, separated by a thin membrane: an upper cell culture chamber and a bottom actuation chamber (Fig. 1(a)). The cell culture chamber is divided into three channels by two rows of hanging posts. The central channel is dedicated to host the cell-laden hydrogel during culture, and its width is defined by the distance between the two rows of posts (300 μm). The side channels (800 μm) serve to provide culture medium to cells, thus mimicking the microvasculature of the native myocardium. The posts have a hexagonal cross-section, whose dimensions and distance were previously optimized.[17] Briefly, the hexagon side length is 28 μm, and the gap between posts of the same row is 50 μm. The actuation chamber consists of a rectangular compartment containing circular posts (radius 30 μm) spaced 200 μm and arranged in two rows 500 μm distant. The device layout was drawn using CAD (AutoCAD, Autodesk Inc.) and the corresponding master molds were fabricated in a clean room environment (PoliFAB, Politecnico di Milano) using a conventional photolithography technique. The layout of each layer was printed at high resolution on a polyester film to create the corresponding photomask that was subsequently used to obtain the negative pattern on a SU8-2050 photoresist (MicroChem, USA) spincoated on 4″ silicon wafers. In particular, the culture chamber master mold was composed of two layers of photoresist (Fig. SI1(a), ESI†): (i) a 50 μm thin layer representing the cell

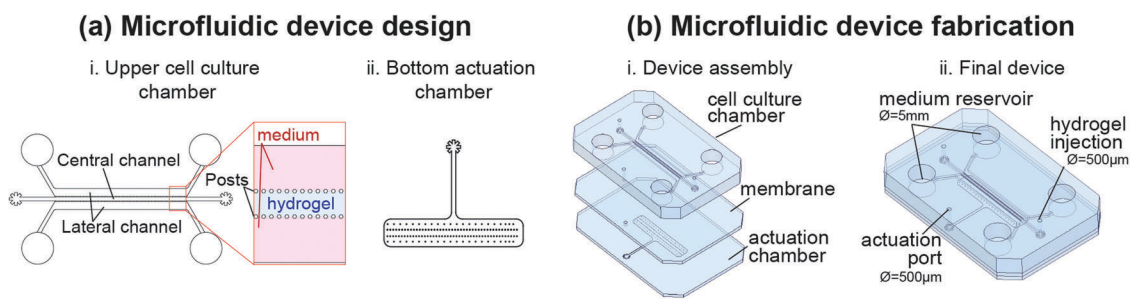

Fig. 1 Microfluidic device design and fabrication. The microfluidic device is composed by a central channel hosting the cell-laden hydrogel and two lateral channels used as culture medium reservoirs (a). The entire device was made of polydimethylsiloxane (PDMS, Sylgard 184, Dow Corning) by mixing in 10 : 1 weight ratio the elastomer base with a curing agent and reticulating at 65 °C for 3 hours. The PDMS membrane thickness was fixed at 1 mm. After curing, PDMS stamps were peeled off the mold and assembled, as sketched in (b), through an air plasma treatment (Harrick Plasma Inc). Prior to the bonding procedure, holes for media reservoir and ports for hydrogel injection were created within the cell culture element through biopsy punchers of 5 mm and 500 μm respectively. Furthermore, a port for the actuation chamber was punched through the cell culture element previously bonded to the membrane. The two layers were finally bonded to the actuation compartment, by carefully aligning it with the central hydrogel portion of the cell culture chamber and the final assembled device was cured overnight at 80 °C to finalize the bonding process.

culture chamber that forms the gap space between pillars and membrane and (ii) a 100 μm thick layer with the post features, creating confinement structures that need to be positioned on top of the previous culture chamber layer. The actuation compartment was conversely obtained by a single photoresist layer, 50 μm thick (Fig. SI1(b), ESI†). The entire device was made of polydimethylsiloxane (PDMS, Sylgard 184, Dow Corning) by mixing in 10 : 1 weight ratio the elastomer base with a curing agent and reticulating at 65 °C for 3 hours. The PDMS membrane thickness was fixed at 1 mm. After curing, PDMS stamps were peeled off the mold and assembled, as sketched in Fig. 1(b), through air plasma treatment (Harrick Plasma Inc.). Prior to the bonding procedure, holes for the media reservoir and ports for hydrogel injection were created within the cell culture element using biopsy punchers of 5 mm and 500 μm respectively. Furthermore, a port for the actuation chamber was punched through the cell culture element previously bonded to the membrane. The two layers were finally bonded to the actuation compartment, by carefully aligning it with the central hydrogel portion of the cell culture chamber and the final assembled device was cured overnight at 80 °C to finalize the bonding process.

2.2 Fibroblast isolation

Neonatal rat fibroblasts were isolated from 2–3 day-old Sprague Dawley rat hearts[18] according to the Swiss Federal guidelines for animal welfare, and the procedure was approved by the Veterinary Office of the Canton Basel (Basel, Switzerland). Briefly, ventricles were digested first overnight in a 0.06% (w/v) solution of trypsin in Hank's balanced salt solution (HBSS, Gibco) and then in a 0.1% (w/v) solution of type II collagenase (Worthington Biochemical Corporation) in HBSS for a series of steps of 4 min at 37 °C and 150 rpm. The cells isolated from 10 hearts were seeded into one polystyrene culture 75 cm^2 flask for 75 min in growth medium (DMEM high glucose supplemented with 10% v/v fetal bovine serum (FBS, HyClone)), 1% v/v penicillin/streptomycin, 1% v/v glutamine, and 1% v/v HEPES (all from Sigma-Aldrich, unless differently claimed). Afterwards, the supernatant was discarded and the adhered fibroblasts were further cultured in a fresh growth medium until 70% confluency and frozen in 10% v/v dimethyl sulfoxide (DMSO), 90% v/v FBS medium and stored in liquid nitrogen.

2.3 Cell culture

Neonatal cardiac fibroblasts were thawed and cultured in monolayers in incubators at 37 °C, 95% humidity and 5% CO_2 using a growth medium (high glucose-Dulbecco's Modified Eagle Medium (DMEM), 10% v/v fetal bovine serum, 1% v/v L-glutamine, 1% v/v HEPES, 1% v/v penicillin–streptomycin) to reach 50–70% confluency. Cells were passaged and dissociated using 0.25% trypsin/1 mM EDTA (Gibco), and resuspended in a growth medium. To generate a microscopic scar tissue-like model, a suspension of fibroblasts was embedded in fibrin hydrogels and injected within microdevices as described previously.[17] Briefly, two separated ice-cold solutions were prepared one containing 20 mg mL^{-1} of fibrinogen, 16 TIU mL^{-1} of aprotinin, 40 mM calcium chloride, and cells at 1.45×10^4 cell per μL in growth medium, and the other containing 5 U mL^{-1} thrombin in phosphate buffered saline (PBS, Sigma-Aldrich). These two solutions were mixed and immediately injected within the central channel of the microdevices (Fig. 1(a)), and kept for 10 minutes in an incubator to promote the complete polymerization of the hydrogel. Hence, the side channels were filled with growth medium supplemented with 1.15 TIU mL^{-1} aprotinin, and fibroblast-laden hydrogels were cultured for 7 days with or without the supplementation of 5 ng mL^{-1} TGFβ1, which is known to support the switch of fibroblasts towards myofibroblasts.[19] The culture medium was changed once a day. To investigate the role of the physiological physical stimuli on myocardial remodelling, the fibrin hydrogels were also mechanically stretched (10% uniaxial strain, frequency 1 Hz[17]) in the presence or absence of 5 ng mL^{-1} TGFβ1 (Fig. 2b). As a control, fibrin-embedded fibroblasts were cultured for 7 days within the microdevices under static conditions (*i.e.* without imposing any mechanical stretching). In summary, the experiment was carried out with four independent experimental groups: with or without TGFβ1 supplementation during static culture (namely, static + TGFβ1 and static-TGFβ1) and with or without TGFβ1 during culture with mechanical stimulation (namely, dynamic + TGFβ1 and dynamic-TGFβ1) (Fig. 2b). Fibroblast proliferation, phenotype switch, matrix deposition and stiffening were evaluated in the different experimental groups (Fig. 2a).

2.4 Immunofluorescence staining

After 2 and 7 days of culture, immunofluorescence analysis was performed directly within the microdevices. The samples were fixed in 4% paraformaldehyde (PFA) for 45 minutes. In order to permeabilize and block non-specific bindings, the samples were incubated for 45 minutes at 4 °C in 5% donkey serum, 2% bovine serum albumin (BSA) and 0.3% Triton (Sigma) in PBS solution. Samples were then incubated overnight at 4 °C with primary antibodies. Cell proliferation was evaluated after 2 days by staining with polyclonal rabbit anti-rat Ki67 (dilution 1 : 100, Abcam). Monoclonal IgG2a anti-mouse alpha-smooth muscle actin (α-SMA, dilution 1 : 400) was used to assess the transition from fibroblast towards myofibroblast phenotype after 7 days of culture. Monoclonal IgG1 anti-mouse collagen type I (dilution 1 : 100, Abcam), polyclonal anti-rabbit aggrecan (dilution 1 : 200, Abcam) and polyclonal anti-rabbit fibronectin (dilution 1 : 200, Abcam) were chosen to define the extracellular matrix (ECM) deposition after 7 days of culture. At every time point, DAPI staining was used to recognise the nuclei. Fluorescently labelled secondary antibodies (Life Technologies) were used at 1 : 200 for 1 hour at room temperature.

2.5 Image analysis

Images of the immunofluorescence-stained samples were acquired using a 20× objective lens on a fluorescence confocal laser scan microscope (Nikon Nala A1) and subsequently analysed by using ImageJ software to quantify cell density, proliferating cells, and cell phenotype switch from fibroblasts towards myofibroblasts (3 replicates per group). Cell density was defined as the total cell number (DAPI count) normalized for the total image area and

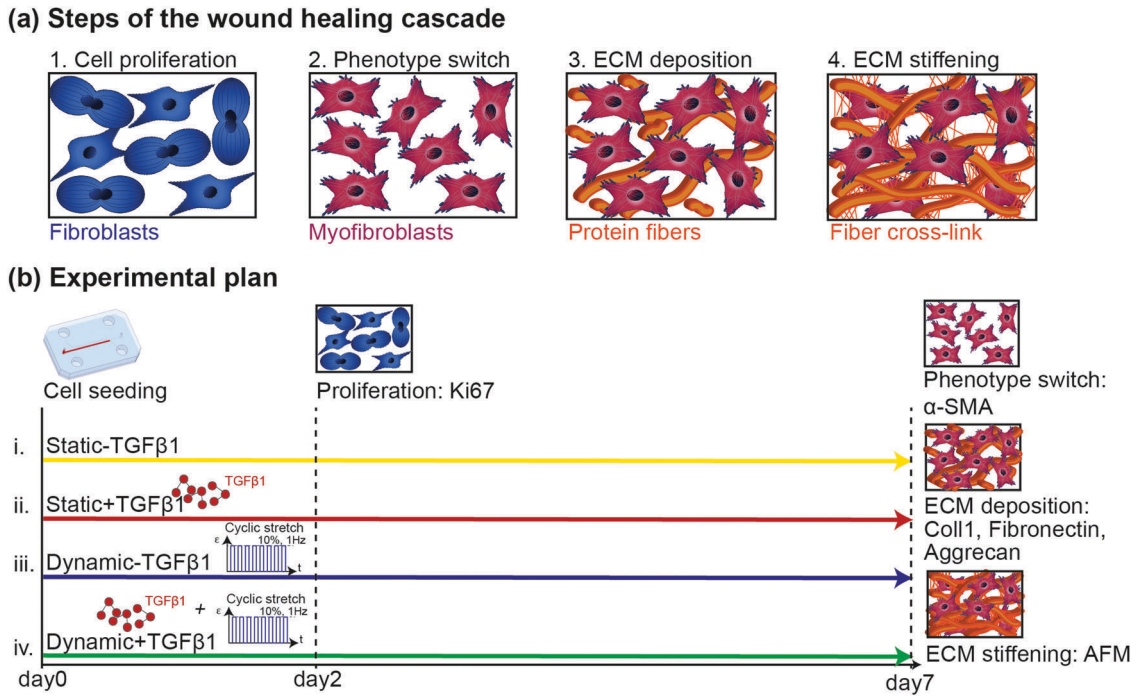

Fig. 2 Description of the wound healing cascade. Experimental plan and description of the 4 conditions.

expressed in cells per mm^2. Proliferating cells were shown as percentage of Ki67-positive cells in the total cell number (DAPI count). Cell phenotype switch was computed as α-SMA-positive cells divided by the total cell number (DAPI count) and expressed in percentage. Representative images of three different regions of each construct were quantified. All data were presented as mean ± standard deviation.

2.6 Quantitative RT-PCR

After 7 days of culture, the produced micro-scar tissues were digested in TRI-Reagent (Sigma) and the total RNA was isolated adapting a previously described method.[20] Omniscript Reverse Transcription kit (Qiagen) was utilized to reverse-transcript cDNA from mRNA at 37 °C for 60 min. Quantitative real-time PCR (qRT-PCR) was performed with TaqMan assays master mix (Life Technologies), using a ABI 7300 RT-PCR system (Applied Biosystems, Carlsbad). *Col1a1* and *Col3a1*, as key markers of the fibrotic tissue, and *Tgfβ1* expressions were investigated. The expression levels of each gene were then normalized using glyceraldehyde-3-phosphate dehydrogenase (*Gapdh*) and calculated using the $2^{\Delta Ct}$ method. Assays on demand have been acquired from Life Technologies.

2.7 Atomic force microscopy (AFM): mechanical characterization

After 7 days of culture, the actuation chamber was carefully removed together with the membrane (Fig. 1(a)), and the top cell culture chamber was then glued upside down onto a plastic culture dish (Sigma-Aldrich) using two components epoxy adhesive (Araldite Rapid, Huntsman Corporation). Measurements were performed in CO_2-saturated culture medium. Atomic force microscopy (AFM) nano-indentation was performed in order to measure the local elastic modulus (*i.e.* Young's modulus) at sub-micron spatial resolution. We used a mechano-optical microscope (MOM), a custom-built AFM that combines AFM (JPK and Nanonis, Specs Zurich GmbH) with a spinning disk confocal system (Visitron AG). For each sample, indentation was performed using a silicon nitride cantilever (HQ CSC38 B, MikroMasch, Nanoworld AG) with a nominal stiffness of 0.03 N m^{-1} and a pyramidal tip of approx. 15 μm in height. The exact spring constant of the cantilever was determined for each cantilever using the thermal tune method.[21] The deflection sensitivity (DS) was determined on the culture dish as reported previously.[22,23] For each experimental group, three different samples were measured and for each sample three force maps in three different random sample locations were recorded. Force maps were recorded at a size of 30 μm × 30 μm and a resolution of 32 × 32 points, thus each force map consisted of 1024 force–displacement curves. Force–displacement curves were corrected for tilt and tip-sample displacement as previously reported[22,23] and the elastic modulus was calculated using the Oliver–Pharr model.[24] An elastic modulus histogram was derived for each experimental group and the corresponding mean and standard deviations were calculated. The elastic modulus values were presented for each experimental group as normalized to the elastic modulus value measured immediately after hydrogel polymerization at day 0.

2.8 Statistical analysis

One-way ANOVA in conjunction with a Bonferroni's multiple comparison test was performed to compare more experimental groups for immunofluorescence quantification and qRT-PCR analysis. A Kruskal–Wallis non-parametric multiple-comparison test

was performed for AFM measurement results. The significant level for all tests was $p < 0.05$. All data are provided as mean ± standard deviation.

3. Results

3.1 Effect of TGFβ1/mechanical stimulation on cell density and proliferation

To assess the capability of the established *in vitro* scar-model to recapitulate the early proliferative stage of wound healing, the effect of TGFβ1 and/or cyclic mechanical loading on cardiac fibroblast proliferation was evaluated. After 7 days, statically cultured constructs showed a similar total number of cells both with ($7.5 \pm 2.8 \times 10^6$ cells per mm^2) or without ($7.1 \pm 1.7 \times 10^6$ cells per mm^2) TGFβ1 (Fig. 3(a)) supplementation. Although no statistically significant difference was found, the cell density slightly increased upon applying a cyclic mechanical stimulation with ($9.44 \pm 2.42 \times 10^6$ cells per mm^2) or without ($10.36 \pm 2.74 \times 10^6$ cells per mm^2) any biochemical conditioning. After 2 days of culture, supplementation of TGFβ1 alone resulted in a statistically significant increase of proliferative fibroblasts from 0.9 ± 0.6% to 3.3 ± 1.2% ($p < 0.005$). Interestingly, also the application of cyclic mechanical stimulation alone was sufficient to increase the cell proliferative activity in a statistically significant manner compared to the static control condition, resulting in an approximately 2-fold increase (static-TGFβ1 0.9 ± 0.6% *vs.* dynamic-TGFβ1 2.4 ± 1.1%) of Ki67-positive cells. The combination of TGFβ1 and cyclic strain further enhanced this effect, leading to 3.7 ± 1.3% Ki67-positive fibroblasts (Fig. 3(b)).

3.2 Effect of TGFβ1/mechanical stimulation on the phenotype switch from fibroblasts to myofibroblasts

First, we assessed whether the cells were positive for cardiac troponin I (data not shown). Under all experimental conditions the cells tested negative, thus excluding that the observed α-SMA positive cells were cardiomyocytes instead of myofibroblasts. Myofibroblasts were present only in low amount in the static culture with a small increase once TGFβ1 was added. Cyclic mechanical stimulation instead increased the number of α-SMA-expressing cells, especially in the region nearby the posts (Fig. 4(a)). Image analysis confirmed the immunofluorescence observations, showing that the static culture without the supplementation of any morphogen factor led to a lower percentage of α-SMA-expressing cells (23.9 ± 15.3%), which increased in the presence of TGFβ1 (43.8 ± 17.5%) (Fig. 4(b)). The application of cyclic mechanical stimulation increased the number of α-SMA-positive fibroblasts with a significant statistical difference compared to static culture (58.5 ± 9% and 56 ± 21% without or with TGFβ1, respectively).

3.3 Effect of TGFβ1/mechanical stimulation on deposition of a scar-like matrix tissue

Although no significant difference was observed among all experimental groups, the supplementation of TGFβ1 showed an increasing trend in the mRNA expression of typical fibrosis markers, namely *Col1a1* and *Col3a1* (3.6- and 1.6-fold increase with respect to the static group without TGFβ1, respectively) (Fig. 5(a) and (b)). Interestingly, the application of a cyclic mechanical stimulation accentuated the observed positive trend by further upregulating *Col1a1* and *Col3a1* expression, independently on TGFβ1 addition. In particular, compared to the static control, *Col1a1* expression was 6.7- and 8.8-times higher in the presence of TGFβ1 and of the sole mechanical stimulation, respectively. *Col3a1* expression showed a similar trend under dynamic conditions compared to the static culture (4.7- and 9.5-fold increase with or without TGFβ1, respectively). The ratio of *Col3a1* and *Col1a1* was also showed to evaluate the conversion in collagen types typically occurring during early stages of scar formation. Upon myocardial infarction, during the early steps of the healing process the newly deposited collagen is mostly type III, later replaced by type I.[25] The ratio of collagen type III/I showed a trend of increase when cyclic mechanical stimulation was applied alone compared to the static culture supplemented with TGFβ1 (Fig. 5(c)). Under static conditions, the supplementation of human recombinant TGFβ1 enhanced the *Tgfβ1* expression (5.2-fold increase). The application of cyclic mechanical stimulation without any exogenous addition of TGFβ1 was alone responsible of an increased expression of *Tgfβ1* (11-fold higher compared to the static control). The combination of mechanical and biochemical stimulation did not further enhance *Tgfβ1* gene expression (Fig. 5(d)). At the protein level the observed results were striking: in cell constructs statically cultured both type-I collagen and aggrecan were positive inside cells with no evident

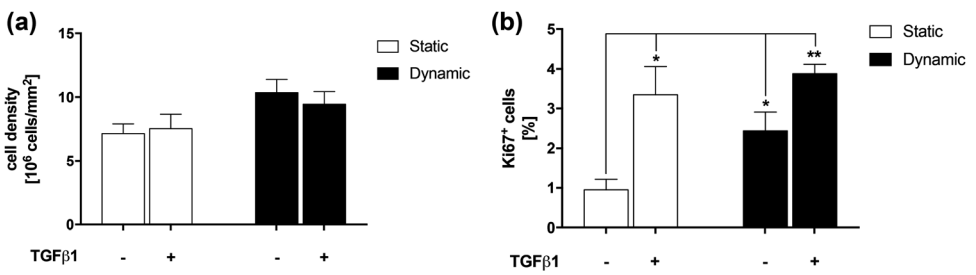

Fig. 3 Cell proliferation. Effect of TGFβ1 and cyclic mechanical stimulation on fibroblast proliferation. (a) Quantification of final cell density (at day 7), defined as the total cell number (DAPI count) normalized for the total image area and expressed in cells per mm^2 ($N = 3$). (b) Quantification of the percentage of Ki67-positive cells, calculated as the ratio between the total number of Ki67+ cells and the total number of cell nuclei ($N = 3$; * = $p < 0.05$; ** = $p < 0.005$).

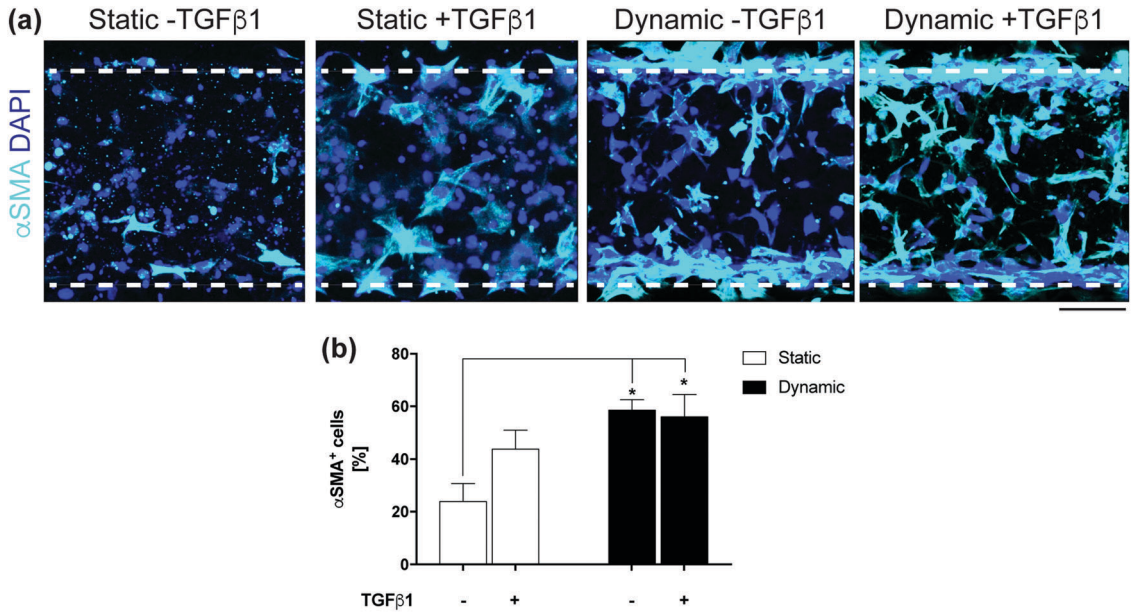

Fig. 4 Fibroblast-to-myofibroblast transition. Role of TGFβ1 and cyclic mechanical stimulation in triggering fibroblast-to-myofibroblast transition. (a) Representative immunofluorescence images of myofibroblasts, identified by α-SMA staining (cyan), after 7 days of culture within the microfluidic platforms. Cell nuclei were stained with DAPI. Scale bar = 100 μm. (b) Quantification of α-SMA+ cells percentage, calculated as the ratio between the total number of α-SMA+ cells and the total number of cell nuclei ($N = 3$; * = $p < 0.05$). All images present two parallel rows of micro-posts located at the top and at the bottom of the field of view, represented by dashed white lines.

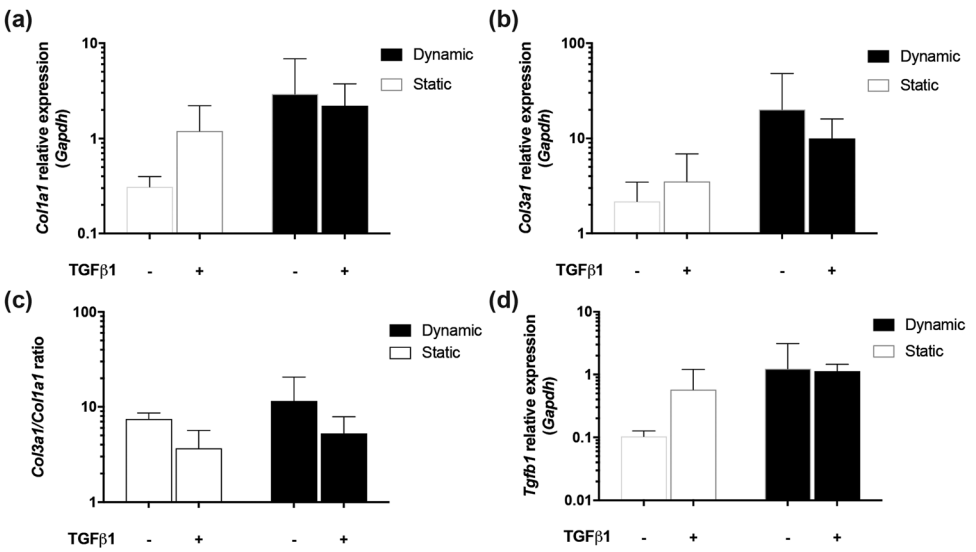

Fig. 5 Fibrosis markers and *Tgfβ1* expression at mRNA level. Real time RT-PCR was performed to assess the mRNA level expressions of type-I (Col1a1) (a) and type-III (Col3a1) (b) collagen, and Tgfβ1 (d) in the four different experimental groups after 7 days of culture within the microfluidic platforms. All ΔCt values are normalized to the relative Gapdh ($N = 3$). The ratio of ΔCt values of Col31 and Col1a1 is also presented (c). No statistical difference was found.

extracellular matrix deposition around the cells (Fig. 6). In contrast to static conditions, the presence of extracellular type-I collagen and aggrecan was also detected upon application of cyclic mechanical stimulation. The combination of cyclic stretching and biochemical stimulation resulted in the formation of abundant deposition of these two proteins uniformly throughout the whole construct. The deposition of fibronectin, instead, was only present in a minor amount around the pillar region under the static-TGFβ1 control condition, and increased by TGFβ1 supplementation, even remaining localized to isolated areas. The application of cyclic mechanical stimulation further enhanced the deposition of the fibronectin-based matrix, enlarging the fibronectin-positive areas. The combination of TGFβ1 and cyclic mechanical stimulation again resulted in a more homogenously distributed deposition of fibronectin throughout the entire construct. Notably for all conditions, areas where fibronectin

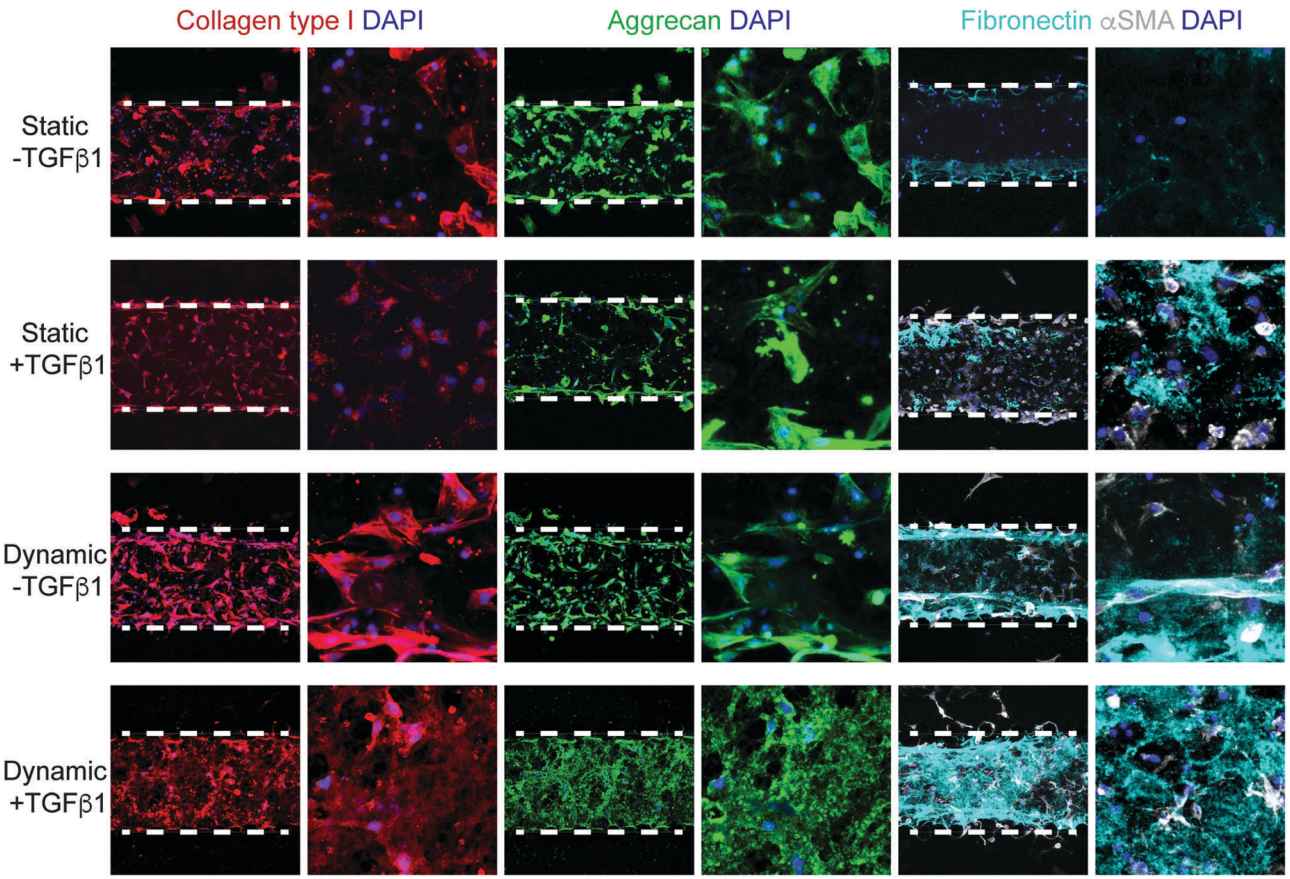

Fig. 6 Extracellular matrix characterization. Representative images at low (left) and high (right) magnification of immunofluorescent staining for type-I collagen (red), aggrecan (green), and fibronectin (cyan) and α-SMA (grey) on the four different experimental groups, after 7 days of culture within the microfluidic platforms. Nuclei were stained with DAPI (blue). Images present the two parallel rows of micro-posts located at the top and at the bottom of the field of view, respectively, and the corresponding higher magnifications. Scale bar = 100 μm.

was secreted mainly overlapped with the ones characterized by a higher α-SMA expressing fibroblast density.

3.4 Effect of TGFβ1/mechanical stimulation on construct stiffening

All the experimental groups presented elastic modulus maps characterized by single peak and symmetrically shaped histograms allowing the extraction of a representative mean local elastic modulus for each indentation map. Each map gave information about the possible local inhomogeneity (Fig. 7(a)). Indeed, it can be shown that the supplementation of TGFβ1 under the static condition contributed to the generation of less homogenous and highly spread local elastic modulus values, compared to a more homogenous local elastic modulus distribution promoted by the sole imposition of the mechanical stimulation (Fig. 7(a) and (b)). For the four experimental groups, map-averaged elastic modulus values were calculated and the stiffness of the constructs after 7 days of culture was presented as fold increase with respect to the elastic modulus of the freshly seeded hydrogels (Fig. 7(c)). After 7 days of culture, the static culture condition without TGFβ1 supplementation was characterized by a small reduction of the elastic modulus compared to the initial condition at day 0 (0.59 ± 0.24-fold increase), with a spread of values comparable to the ones at day 0 (standard deviations: 0.27 and 0.24 at day 0 and 7, respectively). The supplementation of TGFβ1 under static conditions produced very different mechanical properties for each sample and, hence, more dispersed elastic modulus values (1.51 ± 1.46 fold increase/day 0). The imposition of a cyclic mechanical stimulation promoted a significant and reproducible increase of the elastic modulus both in the absence (1.30 ± 0.49 fold increase/day 0) and the presence of TGFβ1 (2.11 ± 0.47 fold increase/day 0) compared to the static negative control (static-TGFβ1).

4. Discussion

In this study, we generated an *in vitro* model, which resembles the fibroblast-mediated scar formation by taking advantage of a multifunctional 3D microscale platform[17] integrating compartments for (i) biochemical and (ii) biomechanical stimulations. Compared to the previous micro-chip version,[17] a novel fabrication method allowed decreasing the layers constituting the device by taking advantage of a multilayer photolithography procedure, therefore, reducing the production time and increasing accuracy during the fabrication phase. Fibroblasts embedded in the fibrin-based constructs were guided *in vitro*

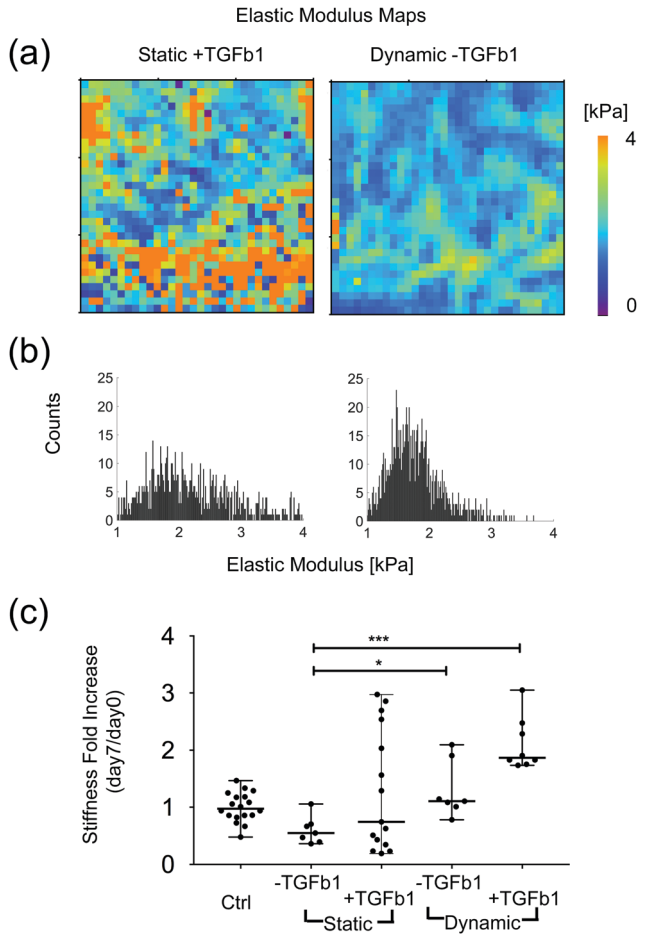

Fig. 7 Mechanical characterization. (a) 30 × 30 μm^2 area indentation maps showing the effect of TGFβ1 supplementation (static + TGFβ1) and mechanical stimulation (Dynamic – TGFβ1) on tissue local elastic modulus and (b) the corresponding elastic modulus histograms. (c) Quantification of stiffness measurements by AFM reveals averaged elastic modulus after 7 days of culture normalized to the elastic modulus of the freshly seeded hydrogels (day 0). Median and range of values are reported for every column of the scatter plot. Notably, all indentations were made far from the pillars, and every indentation point generated a load-displacement curve from which the elastic moduli were calculated. Control group (Ctrl) consists of measurements performed at day 0 = 2.34 kPa. $N \geq 3$; * $p \leq 0.05$, *** $p \leq 0.001$.

towards the recapitulation of some of the key early stages of cardiac wound-healing, namely (i) proliferation, (ii) fibroblast to myofibroblast phenotypic switch, (iii) matrix deposition and (iv) stiffening. As a first consequence of acute myocardial infarction, cardiac fibroblasts are recruited in proximity to the infarcted area and they start to proliferate intensively. The possibility to recapitulate within the microscale platform this early proliferative stage of wound healing was thus firstly assessed. Our results showed that the supplementation of exogenous TGFβ1, both alone and in combination with cyclic mechanical stimulation, contributed to an increase in the final cell density within the model. The fibroblast proliferative activity was particularly stimulated by TGFβ1 supplementation, in accordance with the well-known role of this morphogen in triggering the proliferative stage of the wound-healing process.[8,26] However, also cyclic mechanical stimulation alone was capable of triggering fibroblast proliferation, if compared to the static control without TGFβ1 supplementation. Taken together these observations suggested that both TGFβ1 supplementation and cyclic mechanical loading are effective in stimulating *in vitro* the recapitulation of the early proliferative stage of wound healing.[10] The mechanical stimulation imposition induced a more pronounced phenotypic switch from fibroblast- to myofibroblast-type, determining fibroblast transition and the subsequent expression of contractile proteins such as α-SMA. Nevertheless, the mechanisms responsible for myofibroblast differentiation still remain poorly understood, even though TGFβ1 is known to be critically involved in myofibroblast differentiation.[2,27] Indeed, α-SMA expression was increased by the addition of TGFβ1, but in a lower trend compared to pure mechanical stimulation. This suggests that cyclic mechanical loading alone may play a key-role in triggering the fibroblasts transition to myofibroblasts. However, the importance of TGFβ1 in triggering myofibroblasts to produce ECM proteins was confirmed by an increased trend in the expression of *Col1a1* and *Col3a1*, key-factors typical of the fibrotic tissue.[28] Notably, the application of the cyclic mechanical stimulation further enhanced this effect, independently on TGFβ1 addition. The ratio of *Col3a1* and *Col1a1* also increased upon dynamic stimulation showing a superior accumulation of new collagen, typically thin type III fibers. Type III collagen is typically increased during the early stages of myocardial fibrosis and *in vitro* studies.[29,30] Our experimental setup was, therefore, able to recapitulate also early deposition of collagen fibers typically observed in cardiac diseases.[29] A positive role of cyclic mechanical stimulation in recapitulating a scar-like microenvironment was further confirmed by the analysis of the newly deposited type-I collagen, aggrecan and fibronectin. In the absence of mechanical stimulation, these proteins were mainly characterized by intracellular localization producing a non-homogeneous local elastic modulus along the same tissue, and leading to uneven and highly spread elastic modulus distributions, especially with the supplementation of TGFβ1. This effect may be due to a spatial-wise not uniform remodelling activity along the microdevice channel in the absence of mechanical stimulation.[14] While other *in vitro* models based on the use of scar-stiff hydrogels showed only intracellular collagen expression,[31] in our study, a uniform deposition of ECM components was also fostered by the application of cyclic mechanical stimulation. Interestingly, the predominant role of myofibroblasts in scar-like matrix deposition was confirmed by overlapping secreted fibronectin and α-SMA expressing cells. In fact, differentiated myofibroblasts play the central role in fibrogenesis given their ability to synthesize increased quantities of particular structural ECM proteins, such as collagen type-III, collagen type-I, fibronectin and aggrecan.[2,27] Importantly, this protein synthesis had an effect on the local mechanical stiffness of the constructs, and a more homogeneous localization of these proteins reflected a more homogeneous increase in the local elastic modulus with respect to the initial condition (narrower elastic modulus spread of values). Furthermore, our results showed that the expression of *Tgfβ1* at the gene level is not only activated by exogenous TGFβ1 supplementation, but also by the application of cyclic mechanical loading in the absence of any biochemical stimulus.[4,10] Taken together these results suggest that cyclic mechanical

stimulation promotes TGFβ1 upregulation,[32,33] enhances fibroblast differentiation towards the myofibroblast phenotype[26,34,35] and thus accelerates the formation of a stiffer, more organised and homogenous ECM structure. In previous studies, the mechanical stimulation showed different effects on fibroblast phenotype switch into myofibroblasts: the static stretching showed a clear profibrotic switch of the cardiac fibroblasts only when it was combined to scar-like stiff substrates (*e.g.* around 30 kPa).[5] Interestingly, here we showed that the application of cyclic strain alone was capable of triggering fibrosis even with one order of magnitude softer tissue substrate as fibrin. The difference in the type of mechanical stretching (static *versus* cyclic) and the use of a 3D culture environment might be the possible explanation for the observed results. Our study considers the behaviour of cardiac fibroblasts alone, not taking into account the cross-talk with other cell types, especially cardiomyocytes.[36] This aspect could be a limitation since many studies already demonstrated the importance of investigating bi-directional signalling *via* cell–cell contacts (*e.g.* electrical/mechanical interactions), paracrine factors and ECM[5,35,37] between fibroblasts and cardiomyocytes. However, in most of the previous studies cardiomyocytes were isolated from only healthy tissues and this fact could importantly affect the interpretation of the cellular interactions. Concerning the measures of elastic modulus, these values must not be considered as absolute indication of the construct mechanical properties. The stiffening trend given by the mechanical and biochemical stimulations is intended to complete the more qualitative information obtained by the evaluation of immunofluorescence ECM composition staining. The indentation maps obtained by random location of the indentation area within the constructs gave information about the local elastic modulus, but did not quantitatively describe the differences in terms of the local elastic modulus given by specific ECM proteins. Nevertheless, the measures herein provided can be considered as representative of the effects on the construct maturation given by the four different culture conditions in the experimental groups. Despite the mentioned limitations, the herein proposed microscale device (which might include in the future co-culture of multiple-cells) showed great potential to become an innovative and low-cost screening tool for modelling different wound healing systems, taking advantage of the possible easy implementation of a wide range of physiological mechanical stimulations.

Conflicts of interest

The University of Basel has filed patents related to the AFM technology based on the inventions of M. P., P. Oe. and C. R. M. R. and P. Oc. are among the co-founders of BiomimX S. r. l., and they hold equity in this company.

Acknowledgements

The device manufacture was partially performed at Polifab, the micro- and nanofabrication facility of Politecnico di Milano. This work was partially supported by Fondazione Cariplo, grant no. 2012-0891 (to M. R.) and by the Swiss National Science Foundation Nanotera Project awarded to the PATLiSci II Consortium (to M. P., P. Oe.).

References

1 M. B. Furtado, H. T. Nim, S. E. Boyd and N. A. Rosenthal, *Development*, 2016, **143**, 387.
2 N. A. Turner and K. E. Porter, *Fibrog. Tissue Repair*, 2013, **6**, 5.
3 D. L. Sonin, T. Wakatsuki, K. V. Routhu, L. M. Harmann, M. Petersen, J. Meyer and J. L. Strande, *J. Cardiovasc. Pharmacol. Ther.*, 2013, **18**, 460.
4 G. S. Ugolini, A. Pavesi, M. Rasponi, G. B. Fiore, R. Kamm and M. Soncini, *eLife*, 2017, **6**, e22847.
5 K. M. Herum, J. Choppe, A. Kumar, A. J. Engler and A. D. McCulloch, *Mol. Biol. Cell*, 2017, **28**, 1871.
6 H. Wang, S. M. Haeger, A. M. Kloxin, L. A. Leinwand and K. S. Anseth, *PLoS One*, 2012, **7**, e39969.
7 G. S. Ugolini, M. Rasponi, A. Pavesi, R. Santoro, R. Kamm, G. B. Fiore, M. Pesce and M. Soncini, *Biotechnol. Bioeng.*, 2016, **113**, 859.
8 B. Hinz, *Exp. Eye Res.*, 2016, **142**, 56.
9 A. H. Sadeghi, S. R. Shin, J. C. Deddens, G. Fratta, S. Mandla, I. K. Yazdi, G. Prakash, S. Antona, D. Demarchi, M. P. Buijsrogge, J. P. G. Sluijter, J. Hjortnaes and A. Khademhosseini, *Adv. Healthcare Mater.*, 2017, **6**, 1601434.
10 S. van Putten, Y. Shafieyan and B. Hinz, *J. Mol. Cell. Cardiol.*, 2016, **93**, 133.
11 J. Duan, C. Gherghe, D. Liu, E. Hamlett, L. Srikantha, L. Rodgers, J. N. Regan, M. Rojas, M. Willis, A. Leask, M. Majesky and A. Deb, *EMBO J.*, 2012, **31**, 429.
12 J. G. Travers, F. A. Kamal, J. Robbins, K. E. Yutzey and B. C. Blaxall, *Circ. Res.*, 2016, **118**, 1021.
13 A. Biernacka, M. Dobaczewski and N. G. Frangogiannis, *Growth Factors*, 2011, **29**, 196.
14 V. F. Achterberg, L. Buscemi, H. Diekmann, J. Smith-Clerc, H. Schwengler, J. J. Meister, H. Wenck, S. Gallinat and B. Hinz, *J. Invest. Dermatol.*, 2014, **134**, 1862.
15 M. P. Lutolf and J. A. Hubbell, *Nat. Biotechnol.*, 2005, **23**, 47.
16 J. Sapudom, S. Rubner, S. Martin, S. Thoenes, U. Anderegg and T. Pompe, *Biomater. Sci.*, 2015, **3**, 1291.
17 A. Marsano, C. Conficconi, M. Lemme, P. Occhetta, E. Gaudiello, E. Votta, G. Cerino, A. Redaelli and M. Rasponi, *Lab Chip*, 2016, **16**, 599.
18 M. Radisic, A. Marsano, R. Maidhof, Y. Wang and G. Vunjak-Novakovic, *Nat. Protoc.*, 2008, **3**, 719.
19 R. A. Evans, Y. C. Tian, R. Steadman and A. O. Phillips, *Exp. Cell Res.*, 2003, **282**, 90.
20 P. Chomczynski and N. Sacchi, *Anal. Biochem.*, 1987, **162**, 156.
21 J. Sader, J. W. M. Chon and P. Mulvaney, *Rev. Sci. Instrum.*, 1999, **70**, 3967.
22 M. Loparic, D. Wirz, A. U. Daniels, R. Raiteri, M. R. Vanlandingham, G. Guex, I. Martin, U. Aebi and M. Stolz, *Biophys. J.*, 2010, **98**, 2731.
23 M. Plodinec, M. Loparic, C. A. Monnier, E. C. Obermann, R. Zanetti-Dallenbach, P. Oertle, J. T. Hyotyla, U. Aebi,

M. Bentires-Alj, R. Y. Lim and C. A. Schoenenberger, *Nat. Nanotechnol.*, 2012, **7**, 757.
24 W. C. Oliver and G. M. Pharr, *Journal of Materials Research*, Cambridge University Press, 1992, vol. 7, 1564.
25 H. N. Soufen, V. M. C. Salemi, I. M. S. Aneas, F. J. A. Ramires, A. M. D. Benício, L. A. Benvenuti, J. E. Krieger and C. Mady, *Braz. J. Med. Biol. Res.*, 2008, **41**, 1098.
26 N. G. Frangogiannis, *Antioxid. Redox Signaling*, 2006, **8**, 1907.
27 A. Deb and E. Ubil, *J. Mol. Cell. Cardiol.*, 2014, **70**, 47.
28 L. E. Felkin, E. Lara-Pezzi, R. George, M. H. Yacoub, E. J. Birks and P. J. Barton, *J. Heart Lung Transplant.*, 2009, **28**, 117.
29 B. D. Southern, L. M. Grove, S. O. Rahaman, S. Abraham, R. G. Scheraga, K. A. Niese, H. Sun, E. L. Herzog, F. Liu, D. J. Tschumperlin, T. T. Egelhoff, S. S. Rosenfeld and M. A. Olman, *J. Biol. Chem.*, 2016, **291**, 6083.
30 W. Carver, M. L. Nagpal, M. Nachtigal, T. K. Borg and L. Terracio, *Circ. Res.*, 1991, **69**, 116.
31 J. C. Deddens, A. H. Sadeghi, J. Hjortnaes, L. W. van Laake, M. Buijsrogge, P. A. Doevendans, A. Khademhosseini and J. P. Sluijter, *Adv. Healthcare Mater.*, 2017, **6**, 1600571.
32 L. Buscemi, D. Ramonet, F. Klingberg, A. Formey, J. Smith-Clerc, J. J. Meister and B. Hinz, *Curr. Biol.*, 2011, **21**, 2046.
33 T. Utsunomiya, A. Ishibazawa, T. Nagaoka, K. Hanada, H. Yokota, N. Ishii and A. Yoshida, *Invest. Ophthalmol. Visual Sci.*, 2016, **57**, 6382.
34 R. T. Kendall and C. A. Feghali-Bostwick, *Front. Pharmacol.*, 2014, **5**, 123.
35 D. Pohlers, J. Brenmoehl, I. Löffler, C. K. Müller, C. Leipner, S. Schultze-Mosgau, A. Stallmach, R. W. Kinne and G. Wolf, *Biochim. Biophys. Acta*, 2009, **1792**, 746.
36 J. Pellman, J. Zhang and F. Sheikh, *J. Mol. Cell. Cardiol.*, 2016, **94**, 22.
37 Y. Li, H. Asfour and N. Bursac, *Acta Biomater.*, 2017, **55**, 120.